

Article

# Cutting Performance of Low Stress Thick TiAlN PVD Coatings during Machining of Compacted Graphite Cast Iron (CGI)

Kenji Yamamoto <sup>1</sup>, Majid Abdoos <sup>2</sup>, Jose Mario Paiva <sup>2,3,\*</sup> , Pietro Stolf <sup>2</sup>, Ben Beake <sup>4</sup> , Sushant Rawal <sup>2</sup> , German Fox-Rabinovich <sup>2</sup> and Stephen Veldhuis <sup>2</sup> 

<sup>1</sup> Materials Research Laboratory, Kobe Steel Ltd., Kobe 651-2271, Japan; yamamoto.kenji1@kobelco.com

<sup>2</sup> McMaster Manufacturing Research Institute (MMRI), Department of Mechanical Engineering, McMaster University, Hamilton, ON L8S 4L7, Canada; abdoosm@mcmaster.ca (M.A.); stolfp@mcmaster.ca (P.S.); sushant@mcmaster.ca (S.R.); gfox@mcmaster.ca (G.F.-R.); veldhu@mcmaster.ca (S.V.)

<sup>3</sup> Department of Mechanical and Materials Science, Catholic University of Santa Catarina, Joinville, SC 89203-005, Brazil

<sup>4</sup> Micro Materials Ltd., Wrexham LL13 7YL, UK; ben@micromaterials.co.uk

\* Correspondence: paivajj@mcmaster.ca; Tel.: +1-905-525-9140 (ext. 26450)

Received: 18 December 2017; Accepted: 13 January 2018; Published: 18 January 2018

**Abstract:** A new family of physical vapor deposited (PVD) coatings is presented in this paper. These coatings are deposited by a superfine cathode (SFC) using the arc method. They combine a smooth surface, high hardness, and low residual stresses. This allows the production of PVD coatings as thick as 15  $\mu\text{m}$ . In some applications, in particular for machining of such hard to cut material as compacted graphite iron (CGI), such coatings have shown better tool life compared to the conventional PVD coatings that have a lower thickness in the range of up to 5  $\mu\text{m}$ . Finite element modeling of the temperature/stress profiles was done for the SFC coatings to present the temperature/stress profiles during cutting. Comprehensive characterization of the coatings was performed using XRD, TEM, SEM/EDS studies, nano-hardness, nano-impact measurements, and residual stress measurements. Application of the coating with this set of characteristics reduces the intensity of buildup edge formation during turning of CGI, leading to longer tool life. Optimization of the TiAlN-based coatings composition (Ti/Al ratio), architecture (mono vs. multilayer), and thickness were performed. Application of the optimized coating resulted in a 40–60% improvement in the cutting tool life under finishing turning of CGI.

**Keywords:** TiAlN thick coating; coating process deposition; coating architecture; machining of CGI; coating mechanical properties; FEM

## 1. Introduction

Compacted graphite iron (CGI) has been used in the automotive industry for different applications, including engine blocks, due its improved mechanical properties compared to gray ductile iron. The structure of graphite in CGI makes this alloy strong and stiff with better damping properties, better thermal conductivity, and good castability. CGI has 75% higher strength, 40% higher elastic modulus, and double fatigue strength compared to gray cast iron. The better mechanical properties of CGI originate from its graphite structure and shape, which are vermicular or worm-shaped and randomly oriented. However, the main problem that has prevented this material from being widely used is its poor machinability [1–5].

Experiments have been carried out to compare the machinability of CGI and CI and have shown a great decrease in tool life during machining of CGI [5,6]. Abele et al. [6] and Gastel et al. [7] showed

that using a cubic boron nitride (CBN) cutting tool, the tool life is reduced up to 50% during interrupted cutting and up to 10% during continuous cutting of CGI, and this effect is more significant at higher cutting speeds. Therefore, a cutting speed of 100–120 m/min has been suggested for maximum tool life. It is also reported that difficulties in machining of compacted graphite iron compared to cast iron are due to the very low sulfur content. In machining of cast iron using high speed, sulfur produces a manganese sulfide protective layer on the cutting edge. This protective layer can decrease the abrasive wear of the tool by acting as a lubricant and increase tool life [8,9]. Gastel et al. [7] stated that this protective layer can also protect the tool from oxidation and diffusion at higher cutting temperatures. Heck et al. [5] investigated the tool wear mechanism when machining CGI; they stated that improving machinability of CGI by adjusting its chemical composition is impossible. Therefore, one of these three approaches should be used to improve tool life: (1) improve the cutting materials, (2) use coated inserts at low cutting speeds and high feed rates, and (3) design tools in a way that continuous cutting is replaced by interrupted cutting. With these strategies at hand, many researchers have tried to improve tool life by using hard coatings [2,10–15].

To improve tool life in machining of CGI, Tooptong et al. [12] reported that using a multilayer chemical vapor deposited (CVD) coating of Ti(C,N), Al<sub>2</sub>O<sub>3</sub>, and TiN (Sandvik 3205 and Sandvik 3210) in a turning operation improved tool life by more than 500% at a 250 m/min cutting speed. They also mentioned that using a coated carbide tool could decrease crater wear in the same way. Grzesik et al. [11,16] measured cutting temperature, cutting forces, the coefficient of friction, and surface roughness when turning nodular and CGI with coated and uncoated inserts. The results showed that TiAlN coating successfully decreased cutting forces, the coefficient of friction, and tool-chip contact length. Pavia et al. [2] used TiAlN/TiN, AlCrN, and TiSiN/AlCrN PVD coatings in a drilling operation to improve tool life. Wang [17] compared uncoated and TiAlN-coated inserts in turning of alloyed cast iron. The results showed that TiAlN coating was able to increase tool life and decrease cutting forces.

Based on the previous research, it is well known that hard PVD coatings can improve tool life by protecting the cutting tool surfaces [18]. TiAlN coating has been commercially used for tools since it shows good performance compared to other coatings in terms of tool life [19]. A number of studies have investigated the effect of coating architecture, thickness, and deposition methods on mechanical properties and cutting performance of PVD coatings [20–25]. These studies have shown that the thickness of the PVD coatings is limited by residual stresses caused by the conventional PVD method. A new method of PVD coating deposition, using a so-called “superfine cathode (SFC)” allows deposition of hard PVD coatings as thick as 15–20 μm, which have shown better tool life when compared to the conventional PVD coatings. The TiAlN-based family of coatings is the major coating used in industrial practice for turning operations [26,27]. For that reason, in this research, we selected a thick TiAlN PVD coating, deposited by SFC, to improve tool life in turning of CGI. Performance of thick monolayer and multilayer PVD TiAlN coatings is compared to commercial (5 μm thick) coatings. The properties of the thick coatings are evaluated and tool wear is measured under different cutting conditions.

## 2. Experimental Procedure

In the present study, a family of TiAlN-based coatings with various Al/Ti ratios up to 0.73 have been produced by a cathodic arc ion plating process using an upgraded version of a plasma-enhanced arc fine cathode (FC) [28], named a superfine cathode (SFC). SFC is a magnetically controlled new cathodic arc source, which enables the deposition of a low stress and smooth, thick coating (see the details in Section 4.1).

The AlTiN coatings were deposited by using Ti<sub>0.4</sub>Al<sub>0.6</sub> targets made up by a powder metallurgical process on the polished cemented carbide WC-Co. substrates and Kennametal CNGG432FS turning inserts. To deposit the coatings, an R&D-type hybrid PVD coater (Kobe Steel Ltd., Kobe, Japan) using a SFC (superfine cathode) arc source was employed.

The samples were heated up to 500 °C and soon after the samples were cleaned by means of an Ar-ion etching process. The chamber was pressured with the mixture of gases Ar–N<sub>2</sub>. The total pressure applied to the chamber was 2.7 Pa, being that an N<sub>2</sub> partial pressure of 1.3 Pa. For the coating deposition process, two targets were employed and the parameters were as follows: the arc source was operated at 100 A; a bias voltage of 100 V; a substrate rotation of 5 rpm. The thickness of the coated cutting inserts obtained after the deposition was around 5, 10, and 15 μm.

The crystal structure and preferred orientation of the coating were determined with X-ray diffraction (XRD, Rigaku ULTIMA-PC, Rigaku, Tokyo, Japan), using Cu-k $\alpha$  radiation. The residual stress evaluation was by means of a conventional X-ray diffractometer using the  $\sin^2 \psi$  method. The thickness of the coatings for residual stress measurements was 5 μm. Residual stress measurements were performed using a 2.0 mm round aperture with collection times for each X-ray diffraction peak of about 180 s. The residual stress measurements were performed through the multiple exposure technique with a minimum of 9 $\psi$  angles. This measurement was performed in the plane (101) being the diffraction angle around 44°. For that, a Cu common target was utilized. A Gaussian function was used to fit the diffraction peaks. Ni filters were utilized to suppress fluorescence.

The analyses of the cross-section of the coated samples were done by transmission electron microscopy (TEM) made by JEOL (Tokyo, Japan) (FS2200) equipped with FIB (focused ion beam). In addition, the selected area electron diffraction (SAED) studies were performed as well. The acceleration voltage adjusted at the microscopy was 200 kV. Cemented carbide inserts coated with different PVD coatings were tested for machining of compacted graphite iron (CGI).

To evaluate the wear behavior of the coated inserts, turning experiments were performed on a Nakamura Tome SC450 CNC turning machine. The cutting tests were conducted for finishing operations under the following conditions: cutting speed of 250 m/min, feed rate of 0.34 mm/rev, and depth of cut of 0.25 mm with wet machining. The cutting tests were employed using cemented carbide inserts with TiAlN coatings of different thickness (5, 10 and 15 μm) under wet cutting conditions via a nozzle positioned directly to the cutting tool at a flow rate of 15 L/min. The cutting tests were carried out under finishing operations until the inserts reached the end of tool life, defined as flank wear of 300 μm. During the cutting tests, the tool flank wear was measured using an optical microscope (Keyence-model VHX, KEYENCE America, Elmwood Park, NJ, USA) confirmed. After machining, the rake wear and flank wear on the inserts were investigated by scanning electron microscopy (SEM)/EDS.

The workpiece material—CGI—employed in this work was received as cylindrical bars with 200 mm diameter and 300 mm length. Metallography data on the CGI samples are presented in Figure 1. The optical microscopy inspection revealed that the percentage of nodularity was 68.43% pearlitic. The hardness of the CGI workpiece was 20 HRC.

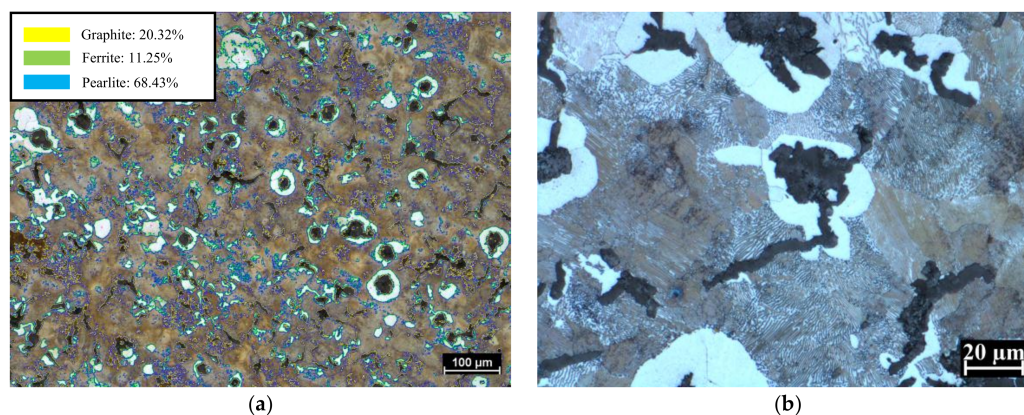


**Figure 1.** Structure of the compacted graphite iron (CGI); optical metallography data: (a) magnification 100 $\times$ ; (b) magnification 500 $\times$ .

The mechanical properties of the coatings were measured through a Micro Materials NanoTest system (Micro Materials Limited, Wrexham, UK). Nanoindentation was performed in order to measure the hardness and elastic modulus of the coatings proposed in this work. The indentation was done through a Berkovich diamond indenter. The load applied was 40 mN and the amount of 40 indentations were performed for each coating. Nano-impact testing was carried out by a NanoTest System. A cube corner indenter was employed during the tests at a frequency of 0.25 Hz. For this frequency, 25 mN of force was applied to produce an impact every 4 s for a total test duration of 100 s. Fracture probability was estimated by ranking the time-to-failure events in order of increasing fatigue resistance and then assigning a probability of failure (Equation (1)):

$$P(f) = n/(N + 1) \quad (1)$$

to the  $n$ th ranked failure event in a total sample size of  $N$ , analogously to the treatment of distributions of failure stresses in Weibull statistics.

### 3. Finite Element Process Modeling

Advances in computational technology have facilitated the access to powerful simulation tools. In this context, the finite element method (FEM) can provide a deeper understanding of the phenomena taking place within the tool/workpiece interface during the machining process. Predictions of factors such as tool wear rates are made possible by the analysis of stress and temperature profiles. The understanding of strain rates, as well as deformation and tribological phenomena, become crucial for the conception of a well-structured simulation model. Severe plastic deformation and dynamic friction conditions provide a high level of complexity to the modeling of machining processes [29]. Another important parameter during machining is the temperature in the cutting zone, which is important to consider during the cutting process [30]. For this paper, temperature and stress profiles were obtained for the machining of CGI under wet cutting conditions, considering the cutting tools coated with TiAlN SFC coatings with different thickness values. The results were then compared to data acquired during the cutting tests.

The modeling was performed using Third Wave Systems AdvantEdge™ simulation software, which associates unconventional finite element models through a Lagrangian formulation, allied to adaptive remeshing capabilities [28], which are appropriate for machining operations. The workpiece material was CGI-pearlitic and the tool substrate was cemented carbide (Grade K313) with a thick TiAlN coating. The parameters and data related to tools adopted during the simulation can be seen in Table 1.

**Table 1.** Cutting parameters applied during the finite element method (FEM).

Operation	Finishing
Cutting Parameters	Feed: 0.34 mm/rev Depth of cut: 0.25 mm (F) Cutting speed: 250 m/min (F) Wet turning via a nozzle positioned directly to the cutting tool Flow rate of 15 L/min Machined length: 5 mm
	Geometry: SNMA120408 Material: Cemented carbide (grade K313) Coating material: TiAlN Coating Thickness: 5, 10, 15 μm
Workpiece	Material: CGI-Pearlitic Dimensions: 75 mm × 20 mm

Mechanical and thermal properties of the materials were acquired according to the FEM program's database. In order to obtain more accurately predicted results, smaller elements (around 0.02 mm) were modeled closer to the tool/chip interfaces, as temperature fields in those regions tend to have a higher influence on tool wear rates. For the remaining sections, a coarser mesh was employed with element sizes ranging around 0.1 mm. The element sizes and temperature conditions are presented in Table 2.

**Table 2.** Cutting parameters applied during FEM.

Element Sizes		Maximum Number of Nodes	No. of Output Frames	Initial Room Temperature
Minimum	Maximum			
0.02 mm	0.1 mm	24,000	30	20 °C

For simplification purposes, the cutting edge was defined ideally as rigid since the main purpose of this work was temperature evaluation and profile stresses on the cutting edge. Simulations were carried out for a total cutting length of 5 mm for each tested condition (5, 10, and 15  $\mu\text{m}$ ), thus allowing the model to reach steady state temperature profiles. A constant friction coefficient was applied to the tool-chip interface according to Coulomb's friction. Also, 100% of the frictional work is considered to be converted into heat.

#### FEM Results

Temperature profiles obtained for the coated cutting tools are presented in Figure 2. By analyzing the gradient in Figure 2d for the 15  $\mu\text{m}$  TiAlN-coated tool, the temperature reduction was more intense when coming from the rake surface into the carbide substrate, compared to the tools coated with thinner layers of the same material (Figure 2e,f). For example, probing the 15  $\mu\text{m}$  sample at a point located 20  $\mu\text{m}$  from the center of its rake surface gave a temperature of 515 °C, whereas probing at the same location for the 5  $\mu\text{m}$  sample resulted in a significantly higher value of 562 °C, meaning that for a 10  $\mu\text{m}$  layer increase, a near 50 °C reduction in temperature was achieved.

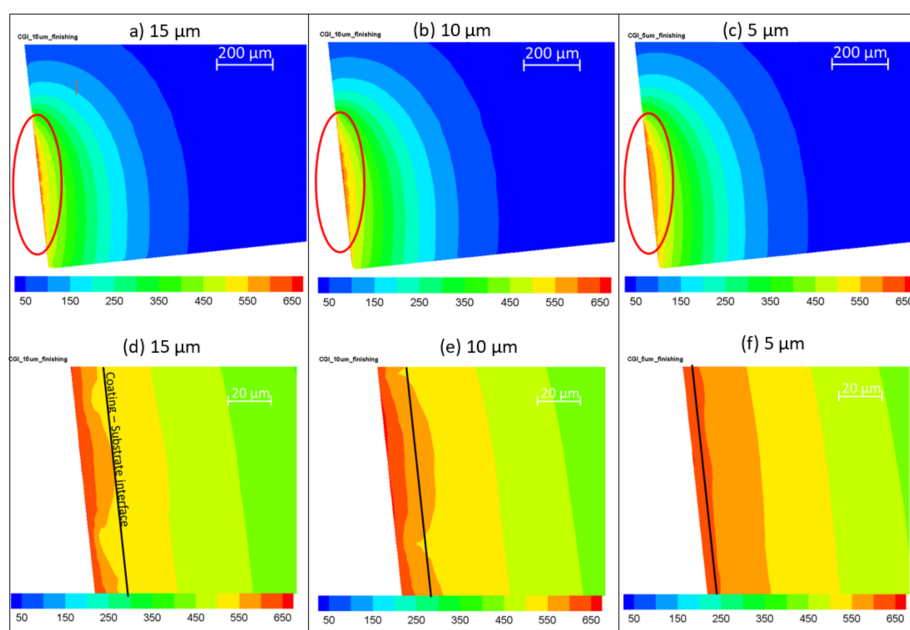


**Figure 2.** Finite element method (FEM) temperature profile for wet machining of CGI using carbide tools with superfine cathode (SFC) TiAlN coatings of different thickness: (a,d) 15  $\mu\text{m}$ , (b,e) 10  $\mu\text{m}$ , and (c,f) 5  $\mu\text{m}$ .

These results show a correlation between coating thickness and heat penetration, supporting the idea that thicker coatings act as thermal insulators for the tool's substrate and should be considered for heat-intensive machining applications, such as CGI turning.

The thick-coated tools compared to the thinly coated tools offer better protection against mechanical and thermal loads, which result in an improvement in wear resistance. In this case, the results from FEM presented in Figure 3 allow us to determine machining-induced effective source stresses present at the cutting edge for different coated tools.

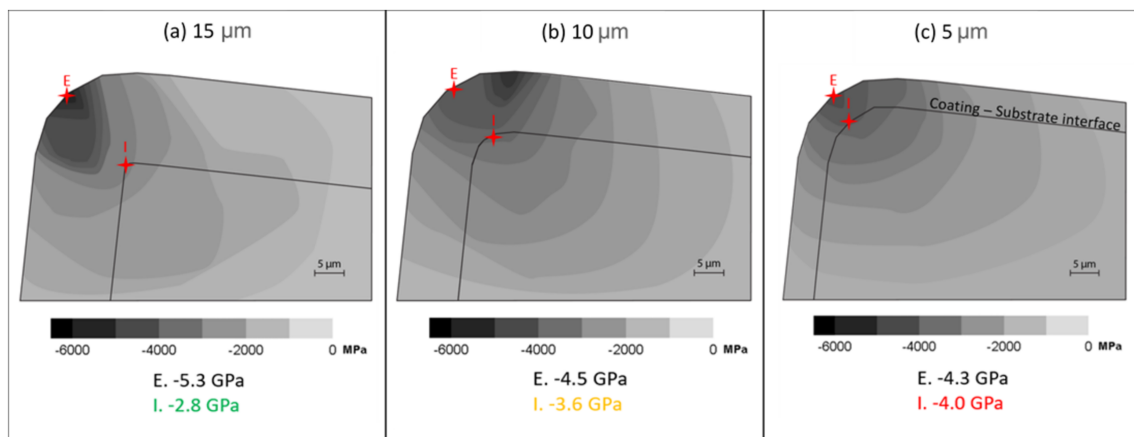


**Figure 3.** FEM stress profile for wet machining of CGI using carbide tools with SFC TiAlN coatings with different thickness: (a) 15  $\mu\text{m}$ , (b) 10  $\mu\text{m}$ , and (c) 5  $\mu\text{m}$ .

The simulation achieved a good correlation for the stresses on the cutting edge versus coating thickness. The maximum equivalent stress for the thick coating, determined by the finite elements method (FEM), reached 5.3 GPa on the cutting edge roundness close to the flank (see Figure 3a), while the thin coating reached 4.3 GPa (Figure 3c). However, the cemented carbide substrate was less stressed for the thick coating than the thin coating. The results show that a thick coating can support more stress during the cutting process and, as a consequence, it helps to reduce the stress that comes into the substrate, which can lead to micro-chipping at the cutting edge and accelerate growth of the wear values [31].

## 4. Results and Discussion

### 4.1. Coating Characterization

TEM/FIB cross-section images of the TiAlN coating deposited by fine cathode (FC) and SFC are presented in Figure 4. The coating has a complex structure that combines a nano-multilayered structure with modulating composition and columnar structure (Figure 4c,d). The HRTEM image of the coating does not show epitaxial growth between the layers. The layers are similar and do not have any preferential orientation as can be seen from the diffraction pattern (Figure 4d).

The surface morphology of the cemented carbide-coated samples was investigated by scanning electron microscopy (SEM, Figure 5a,b) and Alicona (Alicona Imaging GmbH, Raaba, Austria) surface roughness measurements (Figure 5c). The data presented show that SFC provides a smoother surface finish than FC.

XRD data on TiAlN coatings deposited by FC and SFC are presented in Figure 6. It shows that the crystal structure is identical for both FC and SFC coatings (Figure 6a). However, residual stresses varied strongly with the bias voltage applied (Figure 6b) and low stress SFC coatings could be deposited.

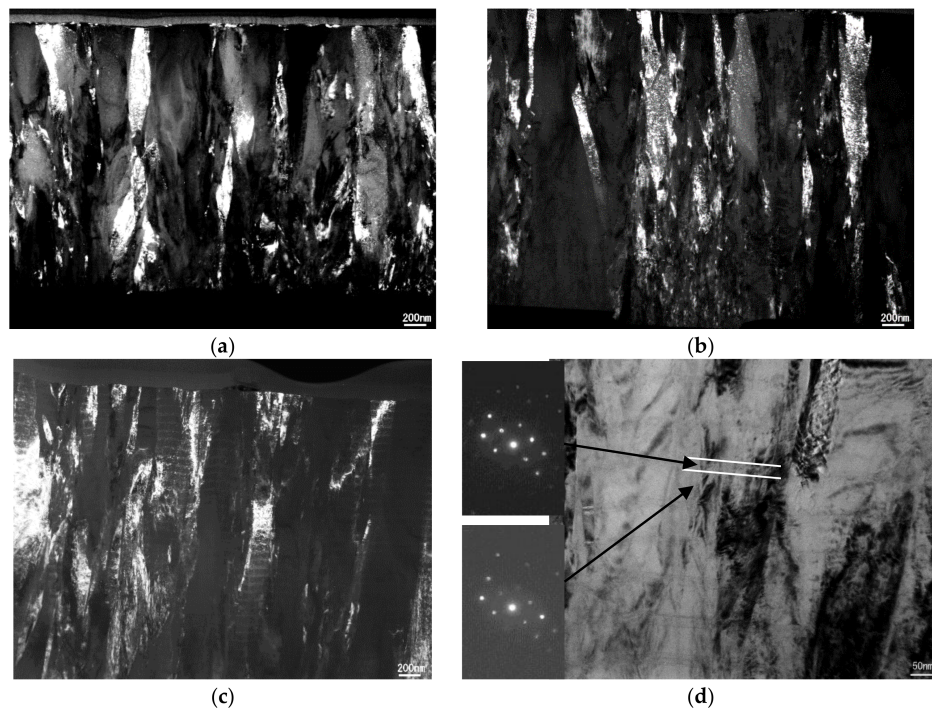


**Figure 4.** Focused ion beam (FIB) TEM data on different TiAlN coatings: (a) thin FC monolayer (thickness of 5 μm); (b) thick SFC monolayer (thickness of 10 μm); (c) thick multilayer (thickness of 10 μm), and (d) HRTEM image of thick multilayer coating (thickness of 10 μm) with the selected area electron diffraction (SAED) pattern inset.

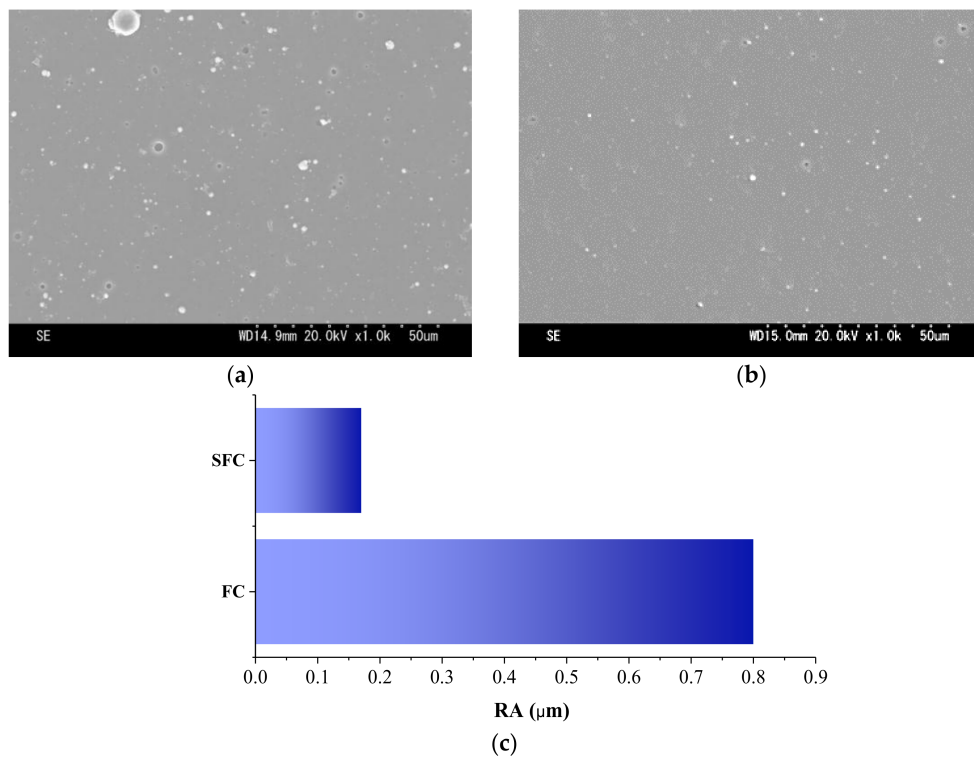


**Figure 5.** Scanning electron microscopy (SEM) data on surface morphology TiAlN coating deposited by FC (a) and SFC (b) plasma sources; (c) comparative surface roughness measurement by Alicona.

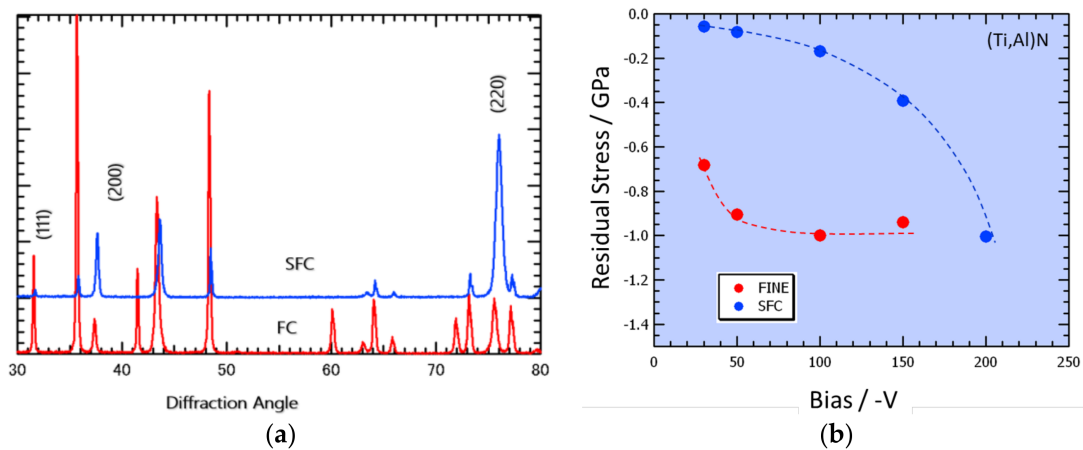


**Figure 6.** XRD data on TiAlN coatings: (a) critical structure of FC vs. SFC coatings; (b) residual stresses vs. bias voltage.

The hardness and related characteristics of the SFC coatings studied are presented in Table 3. The hardness of the coatings is similar. It is worth noting that the multilayer thick coating had greater load support (resistance to plastic deformation) that scaled with the  $H^3/E^2$  ratio. Since the coatings exhibited stochastic time-to-failure behavior in the nano-impact test, the results have been displayed as the cumulative fracture probability within a given test time (Figure 7). When the data are displayed in this way, it can be seen that the multilayer coating also presented lower fracture probability during impact testing as compared to the monolayer (Figure 7). This may be related to its higher  $H^3/E^2$ , which has been shown to improve coating resistance to crack formation by providing enhanced load support.

**Table 3.** Nanomechanical data on SFC  $Al_{60}Ti_{40}N$  coating.

Coating Architecture	Thickness ( $\mu m$ )	Hardness, $H$ (GPa)	Elastic Modulus, $E$ (GPa)	$H/E$	$H^3/E^2$ (GPa)
Monolayer	5	30.6	499.6	0.061	0.115
Monolayer	15	28.1	406.5	0.069	0.134
Multilayer	15	28.7	405.4	0.071	0.143

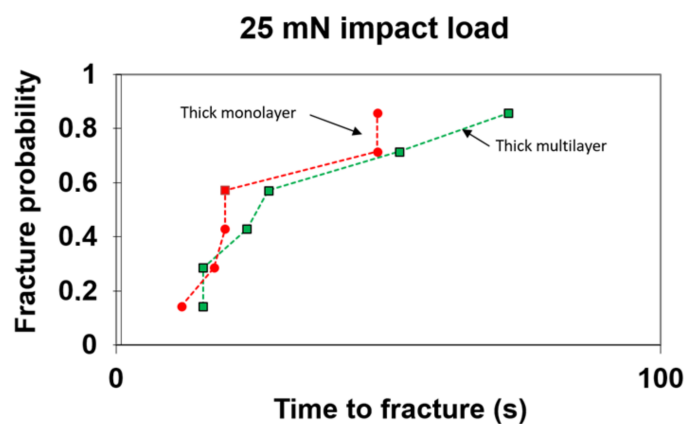


**Figure 7.** Fracture probability of TiAlN mono vs. multilayer coatings, 15  $\mu m$  thick. Frequency is deleted.

#### 4.2. Cutting Tests

The tool life of a number of SFC-deposited TiAlN-based coatings with different compositions was investigated. The data presented in Figure 8 show that the Al/Ti ratio in SFC coatings affect the cutting performance. The tool life was longest within Al/Ti ratio 50–60%. Tool life improvement was around 60% compared to the commercial thin TiAlN coating. When the Al/Ti ratio is higher, the tool life decreases.

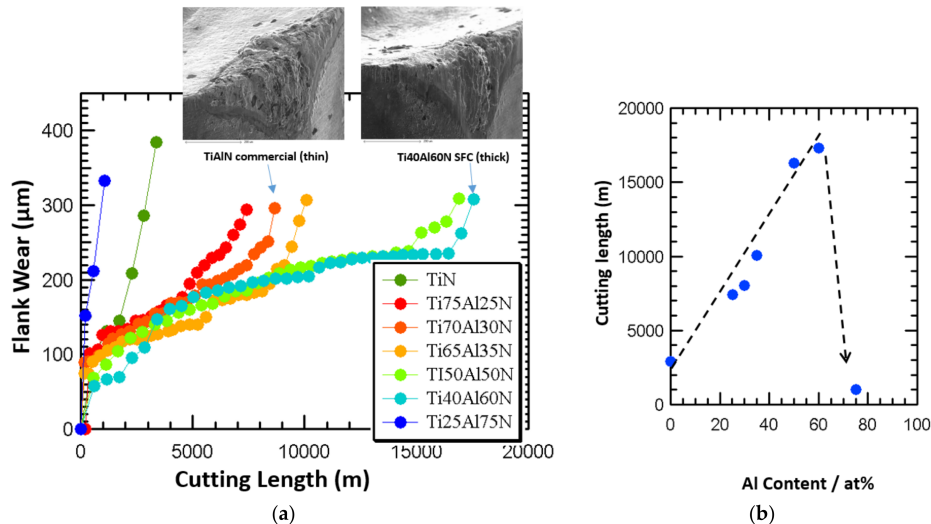


**Figure 8.** Cutting tool life of the TiAlN-based monolayer coatings with different Al/Ti ratios (finishing operation): (a) flank wear vs. length of cut; (b) length of cut vs. Al content. Coatings were deposited by SFC to a thickness of 10 μm. The TiAlN commercial coating is 4–5 μm thick.

SEM images of wear patterns show that during machining of CGI, the buildup edge formation is less intensive on the surface of the cutting insert with the thick coating after a longer length of cut. EDS elemental mapping presented in Figure 9 shows that from the beginning of the wear process the buildup edge formation is more intensive on the surface of thin TiAlN compared to the thick Ti<sub>40</sub>Al<sub>60</sub>N SFC coating.

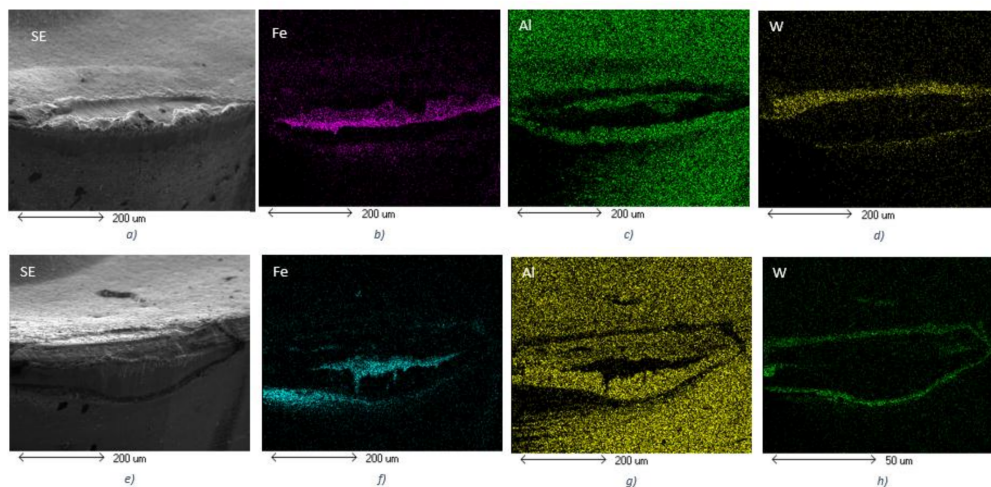


**Figure 9.** EDS elemental maps of the worn cutting tool with TiAlN commercial (thin) coating during machining of CGI (finishing operation) (a–d); and Ti<sub>40</sub>Al<sub>60</sub>N SFC, 10-μm thick coating (e–h). Length of cut is 1000 m.

SFC  $\text{Al}_{60}\text{Ti}_{40}\text{N}$  coatings with various architectures also show noticeable difference in tool life (Figure 10). The tool life was improved by layering bias voltage of thick TiAlN coating (Figure 10). This results in lower fracture probability of the coating layer (Figure 7), which is important for machining of sticky materials with buildup edge formation such as CGI.

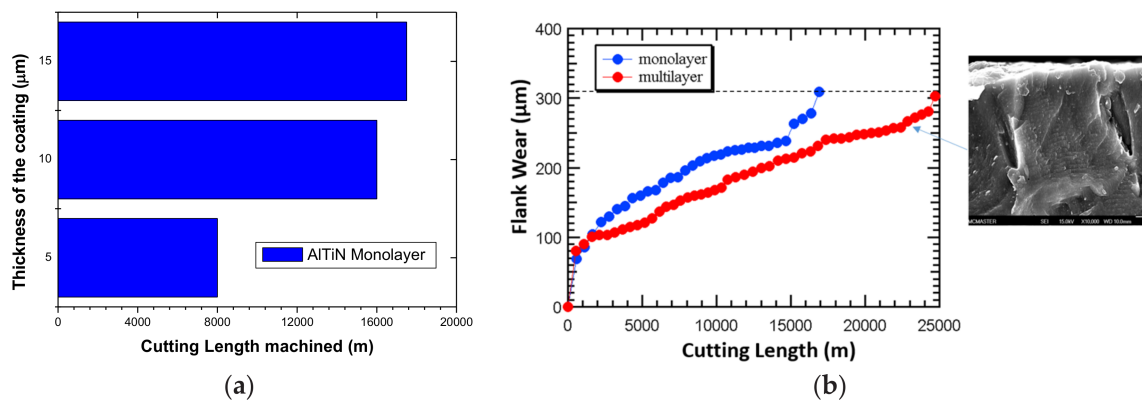


**Figure 10.** (a) Effect of the thickness of monolayer  $\text{Al}_{60}\text{Ti}_{40}\text{N}$  SFC coatings with different thicknesses on tool life during machining of CGI; and (b) effect of multilayer coatings on tool life of  $\text{Al}_{60}\text{Ti}_{40}\text{N}$  SFC coatings (mono- and multilayered, 15  $\mu\text{m}$  thick) during machining of CGI (finishing operation) and SEM fracture section indicating multilayer structure of the coating.

Therefore, the effect of the  $\text{Ti}_{40}\text{Al}_{60}\text{N}$  coating thickness on the tool life was studied. A noticeable increase in the wear performance was shown, which was achieved in monolayer coatings once the thickness grew from 5 to 10  $\mu\text{m}$ . A further increase in thickness (up to 15  $\mu\text{m}$ ) did not result in substantial growth in wear performance. However, a 15- $\mu\text{m}$  thick SFC coating with different architectures showed a noticeable difference on the tool life (Figure 10a,b).

## 5. Conclusions

A new family of PVD coatings deposited by a superfine cathode (SFC) technique combines a smooth surface, the hardness typical for this category of coatings, and low residual stresses. SFC allows the production of hard PVD coatings as thick as 15  $\mu\text{m}$  and above. Data presented show that application of the coatings with the outlined set of characteristics can result in better tool life compared to the conventional PVD coatings for machining of hard to cut materials, particularly compacted graphite iron (CGI). This is accompanied by a lower intensity of buildup formation, which is typical for turning of CGI. Optimization of the TiAlN-based coating composition (Ti/Al ratio), architecture (mono vs. multilayer), and thickness were performed resulting in the cutting tool life improvement.

To support experimental data, a FEM model was built to predict the temperature and stress profiles during wet turning of CGI with a cutting tool with different thicknesses of TiAlN coatings under wet conditions. The FEM model can also give an efficient estimation of the stress state on the tool cutting edge. It shows that the source of stress reaches lower values on the coating/substrate interface for the thick coatings. In addition, FEM modeling shows that the heat flow generated during the cutting is reduced in the cutting tool during machining with a thick coating. The combination of these effects results in an increase in tool life.

The novelty of the results obtained are in the detailed optimization of the characteristics of the newly developed SFC coatings with FEM data on stress/temperature profiles in relation to the wear performance during the machining of hard to cut material such as CGI.

**Acknowledgments:** The authors acknowledge the financial support from the Natural Sciences and Engineering Research Council of Canada (NSERC) and the Canadian Network for Research and Innovation in Machining Technology (CANRIMT). The authors also acknowledge the MMRI for the use of its facilities.

**Author Contributions:** Kenji Yamamoto performed coating synthesis and their structure characterization; Majid Abdoos performed cutting experiments and micro-mechanical properties evaluation; Jose Mario Paiva conceived and designed the FEM modeling for machining of CGI; Pietro Stolf performed FEM modeling; Ben Beake conceived and designed the micro-mechanical measurements; Sushant Rawal performed wear measurements and analyzed the data; German Fox-Rabinovich analyzed the data and co-wrote the paper; Stephen Veldhuis directed the experiments and analyzed the data and co-wrote the paper.

**Conflicts of Interest:** The authors declare no conflict of interest.

## References

1. Mocellin, F.; Melleras, E.; Guesser, W.L.; Boehs, L. Study of the machinability of compacted graphite iron for drilling process. *J. Braz. Soc. Mech. Sci. Eng.* **2004**, *26*, 18–21. [[CrossRef](#)]
2. De Paiva, J.M.F.; Amorim, F.L.; Soares, P.; Torres, R.D. Evaluation of hard coating performance in drilling compacted graphite iron (CGI). *J. Mater. Eng. Perform.* **2013**, *22*, 3155–3160. [[CrossRef](#)]
3. Da Silva, M.B.; Naves, V.T.G.; De Melo, J.D.B.; De Andrade, C.L.F.; Guesser, W.L. Analysis of wear of cemented carbide cutting tools during milling operation of gray iron and compacted graphite iron. *Wear* **2011**, *271*, 2426–2432. [[CrossRef](#)]
4. Sahm, A.; Abele, E.; Schulz, H. Machining of compacted graphite iron (CGI). *Materwiss. Werksttech.* **2002**, *33*, 501–506. [[CrossRef](#)]
5. Heck, M.; Ortner, H.M.; Flege, S.; Reuter, U.; Ensinger, W. Analytical investigations concerning the wear behaviour of cutting tools used for the machining of compacted graphite iron and grey cast iron. *Int. J. Refract. Met. Hard Mater.* **2008**, *26*, 197–206. [[CrossRef](#)]
6. Abele, E.; Sahm, A.; Schulz, H. Wear mechanism when machining compacted graphite iron. *CIRP Ann.-Manuf. Technol.* **2002**, *51*, 53–56. [[CrossRef](#)]
7. Gastel, M.; Konetschny, C.; Reuter, U.; Fasel, C.; Schulz, H.; Riedel, R.; Ortner, H.M. Investigation of the wear mechanism of cubic boron nitride tools used for the machining of compacted graphite iron and grey cast iron. *Int. J. Refract. Met. Hard Mater.* **2000**, *18*, 287–296. [[CrossRef](#)]
8. Diniz, A.E.; Ferrer, J.A.G. A comparison between silicon nitride-based ceramic and coated carbide tools in the face milling of irregular surfaces. *J. Mater. Process. Technol.* **2008**, *206*, 294–304. [[CrossRef](#)]
9. Nayyar, V.; Grenmyr, G.; Kaminski, J.; Nyborg, L. Machinability of compacted graphite iron (CGI) and flake graphite iron (FGI) with coated carbide. *Int. J. Mach. Mach. Mater.* **2013**, *13*, 67–90. [[CrossRef](#)]
10. Fox-Rabinovich, G.S.; Beake, B.D.; Endrino, J.L.; Veldhuis, S.C.; Parkinson, R.; Shuster, L.S.; Migranov, M.S. Effect of mechanical properties measured at room and elevated temperatures on the wear resistance of cutting tools with TiAlN and AlCrN coatings. *Surf. Coat. Technol.* **2006**, *200*, 5738–5742. [[CrossRef](#)]
11. Grzesik, W.; Rech, J.; Zak, K.; Claudin, C. Machining performance of pearlitic-ferritic nodular cast iron with coated carbide and silicon nitride ceramic tools. *Int. J. Mach. Tools Manuf.* **2009**, *49*, 125–133. [[CrossRef](#)]
12. Tooptong, S.; Park, K.H.; Lee, S.W.; Kwon, P.Y. A preliminary machinability study of flake and compacted graphite irons with multilayer coated and uncoated carbide inserts. *Procedia Manuf.* **2016**, *5*, 644–657. [[CrossRef](#)]
13. Souza, J.V.C.; Nono, M.C.A.; Ribeiro, M.V.; Silva, O.M.M.; Lanna, M.A. Turning of compacted graphite iron using commercial TiN coated Si<sub>3</sub>N<sub>4</sub> under dry machining conditions. *Mater. Sci. Forum* **2008**, *591*, 604–609. [[CrossRef](#)]
14. De Oliveira, V.V.; de C. Beltrão, P.A.; Pintaude, G. Effect of tool geometry on the wear of cemented carbide coated with TiAlN during drilling of compacted graphite iron. *Wear* **2011**, *271*, 2561–2569. [[CrossRef](#)]
15. Wang, Q.C.; An, Q.L.; Chen, M.; Liu, G.; Zhang, Y.S. Experimental study on turning of alloy cast iron with coated and uncoated tools. *Adv. Mater. Res.* **2010**, *135*, 265–270. [[CrossRef](#)]
16. Grzesik, W.; Zak, K. Mechanical, thermal and tribological aspect of the machining process of nodular iron with coated carbide and ceramic tools. *Adv. Manuf. Sci. Technol.* **2009**, *33*, 31–43.
17. Wang, J. Effect of the multi-layer surface coating of carbide inserts on the cutting forces in turning operations. *J. Mater. Process. Technol.* **2000**, *97*, 114–119. [[CrossRef](#)]
18. Bouzakis, K.D.; Michailidis, N.; Skordaris, G.; Bouzakis, E.; Biermann, D.; M'Saoubi, R. Cutting with coated tools: Coating technologies, characterization methods and performance optimization. *CIRP Ann.-Manuf. Technol.* **2012**, *61*, 703–723. [[CrossRef](#)]

19. Jindal, P.C.; Santhanam, A.T.; Schleinkofer, U.; Shuster, A.F. Performance of PVD TiN, TiCN, and TiAlN coated cemented carbide tools in turning. *Int. J. Refract. Met. Hard Mater.* **1999**, *17*, 163–170. [[CrossRef](#)]
20. Avelar-Batista, J.C.; Spain, E.; Housden, J.; Fuentes, G.G.; Rodriguez, R.; Montalá, F.; Carreras, L.J.; Tate, T.J. Effect of coating thickness and deposition methods on the stripping rate of Cr–N coatings. *Surf. Coat. Technol.* **2005**, *200*, 1842–1848. [[CrossRef](#)]
21. Carvalho, S.; Rebouta, L.; Ribeiro, E.; Vaz, F.; Denannot, M.F.; Pacaud, J.; Rivière, J.P.; Paumier, F.; Gaboriaud, R.J.; Alves, E. Microstructure of (Ti,Si,Al)N nanocomposite coatings. *Surf. Coat. Technol.* **2004**, *177–178*, 369–375. [[CrossRef](#)]
22. Bouzakis, K.-D.; Hadjiyiannis, S.; Skordaris, G.; Mirisidis, I.; Michailidis, N.; Erkens, G. Wear development on cemented carbide inserts, coated with variable film thickness in the cutting wedge region. *Surf. Coat. Technol.* **2004**, *188–189*, 636–643. [[CrossRef](#)]
23. Bouzakis, K.-D.; Hadjiyiannis, S.; Skordaris, G.; Mirisidis, I.; Michailidis, N.; Koptsis, D.; Erkens, G. Milling performance of coated inserts with variable coating thickness on their rake and flank. *CIRP Ann.* **2004**, *53*, 81–84. [[CrossRef](#)]
24. Bouzakis, K.-D.; Hadjiyiannis, S.; Skordaris, G.; Anastopoulos, J.; Mirisidis, I.; Michailidis, N.; Efstathiou, K.; Knotek, O.; Erkens, G.; Cremer, R.; et al. The influence of the coating thickness on its strength properties and on the milling performance of PVD coated inserts. *Surf. Coat. Technol.* **2003**, *174–175*, 393–401. [[CrossRef](#)]
25. Vereschaka, A.A.; Grigoriev, S.N. Study of cracking mechanisms in multi-layered composite nano-structured coatings. *Wear* **2017**, *378–379*, 43–57. [[CrossRef](#)]
26. Wang, D.-Y.; Li, Y.-W.; Ho, W.-Y. Deposition of high quality (Ti,Al)N hard coatings by vacuum arc evaporation process. *Surf. Coat. Technol.* **1999**, *114*, 109–113. [[CrossRef](#)]
27. Munz, W.-D.M. Ti-Al nitride films: A new alternative to TiN coatings. *J. Vacuum Sci. Technol.* **1986**, *4*, 2717–2725. [[CrossRef](#)]
28. Yamamoto, K.; Sato, T.; Takahara, K.; Hanaguri, K. Properties of (Ti,Cr,Al)N coatings with high Al content deposited by new plasma enhanced arc-cathode. *Surf. Coat. Technol.* **2003**, *174*, 620–626. [[CrossRef](#)]
29. Shaw, M.C. *Metal Cutting Principles*, 2nd ed.; Oxford University Press: Oxford, UK, 2005.
30. Melkote, S.N.; Grzesik, W.; Outeiro, J.; Rech, J.; Schulze, V.; Attia, H.; Arrazola, P.J.; M'Saoubi, R.; Saldana, C. Advances in material and friction data for modelling of metal machining. *CIRP Ann.-Manuf. Technol.* **2017**, *66*, 731–754. [[CrossRef](#)]
31. Grzesik, W. Determination of temperature distribution in the cutting zone using hybrid analytical-FEM technique. *Int. J. Mach. Tools Manuf.* **2006**, *46*, 651–658. [[CrossRef](#)]



© 2018 by the authors. Licensee MDPI, Basel, Switzerland. This article is an open access article distributed under the terms and conditions of the Creative Commons Attribution (CC BY) license (<http://creativecommons.org/licenses/by/4.0/>).